# Ubiquitin in Motion: Structural Studies of the Ubiquitin-Conjugating Enzyme~Ubiquitin Conjugate

**ARTICLE** *in* BIOCHEMISTRY · FEBRUARY 2011

Impact Factor: 3.02 · DOI: 10.1021/bi101913m · Source: PubMed



**5 AUTHORS**, INCLUDING:

Kate E Stoll
University of Washington Seattle
**5** PUBLICATIONS **180** CITATIONS

SEE PROFILE

Published in final edited form as:
*Biochemistry*. 2011 March 15; 50(10): 1624–1633. doi:10.1021/bi101913m.

# Ubiquitin in Motion: Structural studies of the E2~Ub conjugate

**Jonathan N. Pruneda**[1,†], **Kate E. Stoll**[1,2,†], **Laura J. Bolton**[1], **Peter S. Brzovic**[1], and **Rachel E. Klevit**[1,2]

[1]Department of Biochemistry, at the University of Washington, Seattle, Washington, 98195

[2]Biomolecular Structure and Design Program, at the University of Washington, Seattle, Washington, 98195

## Abstract

Ubiquitination of proteins provides a powerful and versatile post-translational signal in the eukaryotic cell. The formation of a thioester bond between ubiquitin (Ub) and the active site of a ubiquitin-conjugating enzyme (E2) is critical for Ub transfer to substrates. Assembly of a functional ubiquitin ligase (E3) complex poised for Ub transfer involves recognition and binding of an E2~Ub conjugate. Therefore, full characterization of the structure and dynamics of E2~Ub conjugates is required for further mechanistic understanding of Ub transfer reactions. Here we present characterization of the dynamic behavior of E2~Ub conjugates of two human enzymes, UbcH5c~Ub and Ubc13~Ub, in solution as determined by NMR and SAXS. Within each conjugate, Ub retains great flexibility with respect to the E2, indicative of highly dynamic species that adopt manifold orientations. The population distribution of Ub conformations is dictated by the identity of the E2: UbcH5c~Ub populates an array of extended conformations and the population of Ubc13~Ub conjugates favors a closed conformation in which the hydrophobic surface of Ub faces Helix 2 of Ubc13. We propose that the varied conformations adopted by Ub represent available binding modes of the E2~Ub species and thus provide insight into the diverse E2~Ub protein interactome, particularly regarding interaction with Ub ligases.

### Keywords

ubiquitin; ubiquitin conjugating enzyme; ubiquitination; UbcH5; Ubc13; NMR; spin label; SAXS

Covalent attachment of the 8.6 kDa Ubiquitin (Ub) to target proteins is an essential step in eukaryotic signaling pathways. The type of Ub modification can vary, inducing distinct signals. For example, mono-ubiquitination may elicit a signal for protein transport while poly-ubiquitination (attachment of a chain of Ubs to the target) may mark a protein for proteasome-mediated degradation. Covalent attachment of Ub to a substrate proceeds through a multi-enzyme process consisting of a Ub-activating enzyme (E1), a Ub-conjugating enzyme (E2), and a Ub ligase (E3) (1). The human genome contains two Ub E1s, ~35 E2s, and many hundreds of E3s (2). Despite the large number of E2s, they share significant similarity at both the sequence and structure levels. The E2 plays a central role in the ubiquitination cascade, shuttling Ub from an E1 to an E3/substrate complex. The E2

Address correspondence to: Rachel Klevit University of Washington Box 357350, Seattle, Washington 98195. Telephone: 206-543-5891 Fax: 206-543-8394 klevit@uw.edu.
†These authors contributed equally to this work.

**Supporting Information Available**

Specific protein residues affected by PRE and CSP, as well as SAXS statistics, and E2 sequence alignments are listed in supporting information. This material is available free of charge via the Internet at http://pubs.acs.org.

holds Ub in its activated form *via* formation of a thioester bond between the carboxy-terminus of Ub and the E2's active site cysteine (denoted as E2~Ub).

The small size and high solubility of many E2s have made them prime candidates for structural investigations. There are ~100 structures of E2s in the Protein Data Bank (PDB) and 23 of the ~35 human E2s have their structures deposited. This wealth of information reveals that all E2s are related by their conserved catalytic cores which fold into an α/β topology. Significantly fewer structures of E2~Ub complexes have been solved, due probably to the technical challenges that the labile thioester conjugate poses. There are presently five structures of E2~Ub conjugates or close structural analogs that have been determined by X-ray crystallography or NMR: Ubc13~Ub (PDB code 2GMI) (3); Ubc1~Ub (PDB code 1FXT) (4); UbcH8~Ub (PDB code 2KJH) (5); and UbcH5b~Ub (PDB codes 3A33 (6), and 3JW0 (7)). In each case, the backbone of the E2 and Ub moieties are not significantly altered from their free structures. However, each structure presents a unique relative orientation of the E2 and Ub units.

Despite the wealth of atomic-level structural information on E2s, on E2/E3 complexes, and a growing number of E2~Ub conjugates, the ways in which E3s catalyze Ub transfer from an E2~Ub remain poorly understood. It is clear that one function of the E3 is to bind a substrate simultaneously with binding an E2~Ub, thereby bringing the two components into proximity. However, even in the absence of a protein substrate, E3s have been shown to enhance the rate at which Ub is released from an E2~Ub conjugate, presumably due to reaction of the thioester bond with solvent or buffer components (8) (9). Although this so-called hydrolysis or release rate may not be the mechanistic equivalent of the reaction involving a substrate lysine side chain, the ability of an E3 to enhance the reactivity of an E2~Ub suggests that an E2 active site can somehow be tuned in response to E3 binding. As a step towards understanding how an E3 ligase regulates E2~Ub activity, a more complete description of the E2~Ub conjugate is needed. Furthermore, the *in vivo* steady-state equilibrium of the human E2 Ubc2b favors the conjugated form and this is likely a general feature of E2s because E1 is efficient at maintaining E2s in the conjugated state (10) (11). Thus, E3s and other cellular proteins are more likely to encounter E2~Ubs than free E2s. We have chosen to focus on UbcH5c and Ubc13, two highly related E2 enzymes (45.6% sequence identity and 61% similarity) with divergent activities and specificities (Figure S3). Orthologues of both UbcH5c and Ubc13 play key roles in all organisms from yeast to human (12). These two E2s are well characterized, with structures determined for each in their free and Ub-conjugated states (Ubc13 PDB IDs 1J7D (13), 2GMI; UbcH5 PDB IDs 1X23, 3A33), both alone and in complex with interacting proteins. These studies and our own make use of an active site Cys-to-Ser mutation to generate a more stable oxyester-linked E2-O~Ub. In this study, we use NMR chemical shift mapping, site-specific paramagnetic labeling, and small angle X-ray scattering (SAXS) to examine the ensemble of E2~Ub conformations populated by UbcH5c~Ub and Ubc13~Ub in solution. Characterization of the E2~Ub conjugate in solution will facilitate future structural studies with interacting proteins, including E3 ligases.

## EXPERIMENTAL PROCEDURES

### Plasmids, Protein Expression, and Purification

N-terminal $His_6$-tagged Ubc13 was expressed from the pET24 vector. UbcH5c was expressed from the pET28N vector. UbcH5c and BRCA1_1–112/BARD1_25–139 were purified as previously described (14). Proteins were expressed in *E. coli* (BL21 star DE3 cells) at 37°C, and induced with 1mM IPTG for four hours, or at 16°C induced with 200 μM IPTG for 18 hours. $His_6$-Ubc13 was purified using a $Ni^{2+}$ affinity column, followed by size

exclusion chromatography on SDX75 resin in 25 mM sodium phosphate, 150 mM NaCl buffer at pH 7.0, the buffer used for all NMR experiments.

### Spin Label Modification

Four mutant forms of Ub were generated using site-directed mutagenesis (K11C, D39C, K48C, K63C) to incorporate a cysteine for chemical modification with the thiol-reactive relaxation probe 4-(2-Iodoacetamido)-TEMPO (Sigma-Aldrich) to form a covalently-linked, non-transferable adduct. Reactions between TEMPO and each cysteine mutant of Ub were performed at 25°C overnight in a 1:5 Ub:TEMPO molar ratio. Reaction yields were quantified by MALDI-MS; in all cases the reaction went essentially to completion (>95%). Unreacted TEMPO was removed by dialysis prior to the conjugation reaction. Paramagnetic activity was confirmed by incorporating a spin label into $^{15}$N-Ub K63C and collecting HSQC spectra before and after reducing the nitroxide probe with ascorbate. Comparison of the $^{15}$N-Ub K63SL ascorbate-reduced spectrum with wildtype Ub showed little spectral perturbation associated with the cysteine mutation and subsequent modification with the spin label.

### Formation of the E2~Ub conjugate

To characterize the conjugated forms of the E2s UbcH5c and Ubc13, we used an active site Cys-to-Ser mutation (C85S in UbcH5; C87S in Ubc13) to generate an oxyester between the C-terminus of Ub and the E2. The resulting bond is only one atom different than the wildtype thioester and significantly more stable. All structural work described in this study utilized the active site Cys-to-Ser mutation; the conjugates formed with these E2s are denoted as E2-O~Ub. NMR studies of the UbcH5c-O~Ub conjugate were performed in the context of the S22R mutation to prevent non-covalent Ub binding (15). $^{15}$N E2-O~Ub oxyester conjugates were generated by reaction of 5–10 μM E1, 600 μM TEMPO-modified or wildtype Ub, 300 μM $^{15}$N E2s ($^{15}$N C85S-S22R-UbcH5c or $^{15}$N C87S-Ubc13), 5 mM $MgCl_2$, and 2.5 mM ATP at 30°C for 3 to 6 hours. E2-O~Ub conjugates were purified from unreacted material by gel filtration on SDX75 resin and homogeneity of the E2-O~Ub species was confirmed by SDS-PAGE. 2D ($^1$H, $^{15}$N)-TROSY-HSQC spectra were collected on samples containing 150 μM E2~Ub before and after reduction of the paramagnetic probe with 5 molar equivalents of ascorbate.

### NMR Spectroscopy

Chemical shift perturbation and paramagnetic relaxation enhancement (PRE) data were collected at 25°C on a Bruker 500 MHz AVANCE II NMR spectrometer (University of Washington). Relaxation data were collected at 25°C on a Varian 600 MHz INOVA NMR spectrometer (Pacific Northwest National Labs). Data processing and analysis were performed using NMRPipe (16) and NMRView (17). Peak intensities were measured in NMRView and intensity ratios for individual NH peaks in the active and ascorbate-reduced spectra ($I/I_{red}$) were calculated. Spin label-affected E2 resonances were identified as those with a peak intensity ratio below 0.70. In general, this cutoff was approximately one standard deviation from the mean. Chemical shift perturbations observed by 2D TROSY-HSQC NMR were quantified in ppm with the equation $\Delta\delta_j=((\Delta\delta_j{}^{15}N/5)^2+(\Delta\delta_j{}^{1}H)^2)^{1/2}$.

### Small Angle X-ray Scattering

SAXS data were collected at the Stanford Synchrotron Radiation Lightsource beamline 4-2. Data were collected for UbcH5c, UbcH5c~Ub, and $His_6$-Ubc13~Ub at 10, 5, and 0.5 mg/mL concentrations in 25mM sodium phosphate, 150mM NaCl, 2mM DTT (free radical scavenger), pH 7.0 at 25°C. Data on $His_6$-Ubc13 was collected at 7, 5, and 0.5 mg/mL in the same buffer without DTT. Initial data subtraction and averaging was performed with SSRL

in-house software and confirmed using PRIMUS (18). $R_g$ values calculated from the Guinier plot, the Porod plot, and the P(r) function were all consistent. The P(r) functions were calculated using GNOM (19) and theoretical scattering profiles of published structures were calculated using CRYSOL (20) and OLIGOMER (18). Existing E2~Ub structures were substituted with the appropriate E2 structure prior to calculation of the theoretical scattering profile. Flexibility analysis using the ensemble optimization method (EOM) (21) was performed using RanCh to create a pool of 10,000 random E2~Ub conformations based upon flexibility in Ub residues 72–76. The GAJOE genetic algorithm was used as described previously to select an ensemble of 20 conformations that, together, best fit the scattering data (21). SAXS data for free $His_6$-Ubc13 was used to model a single conformation of the $His_6$-tag that is consistent with the measured SAXS curve. The His-tag model was then used to represent the Ubc13 component within the His-Ubc13~Ub RanCh/GAJOE analysis.

## RESULTS

We have previously reported the NMR chemical shift perturbations observed for UbcH5c-O~Ub relative to the free protein counterparts (15). The most notable feature of the UbcH5-O~Ub conjugate was its asymmetric perturbations in which significant chemical shift perturbations were observed to emanate away from the active site in the E2 but were highly localized to the extreme C-terminus of the Ub moiety. Ub chemical shifts beyond the C-terminal residues are small (<0.05 ppm). While over one third (45/126) of UbcH5c resonances are shifted by greater than one peakwidth, only twelve are shifted by greater than one standard deviation from the mean. Mapping these twelve residues onto the 3-dimensional structure reveals a spotted surface spanning the crossover helix (Helix-2), active site, Loop 5 (residues 75–77), and the C-terminal helices (helices 3 and 4) (see figure 3C in reference 15). Such a distributed perturbation surface is consistent with either a conformational adjustment in interior hydrophobics (aromatics) or a dynamic UbcH5c-O~Ub species in which activated Ub makes transient contact with multiple E2 surfaces.

### Mapping the Ubc13~Ub interface by Chemical Shift Perturbation Analysis

To allow for study of the Ubc13-O~Ub conjugate by NMR, the 2D HSQC-TROSY spectrum of $^{15}$N-Ubc13-O~Ub was assigned. The lifetime of the Ubc13-O~Ub species in solution is too short for collection of 3D spectra such as HNCA or HNCACB. Based on the observation that E2 structures do not change significantly in their Ub-conjugated states (3) (6) (5), we turned to HNCO spectra which can be collected in shorter acquisition times. The chemical shifts of backbone carbonyl groups are largely determined by the structure in which they are found, so the spectrum of conjugated Ubc13 could be assigned by matching HNCO carbonyl assignments between free and conjugated Ubc13 (Table S1). Comparison of the $^{1}$H$^{15}$N chemical shifts of the free and conjugated protein reveals significant chemical shift perturbations (CSPs) in backbone amide resonances beyond the active site of Ubc13 (Figure 1A, C). In contrast to UbcH5-O~Ub, $^{15}$N-Ub exhibits significant CSPs beyond its C-terminal tail when conjugated to Ubc13 (Fig 1B, C, D).

When mapped onto the crystal structure of Ubc13-O~Ub (PDB ID 2GMI), the CSPs resulting from the conjugation of Ub to Ubc13 reveal discrete surfaces on each protein component. The surface on Ubc13 is comprised of Helix-2 (“crossover helix”; residues 100–114), Loop 8 (residues 114–123) and, to a smaller extent, the penultimate C-terminal helix (See Table S2 for residue-level information). The I44 hydrophobic surface of Ub is perturbed upon conjugation to Ubc13 (Figure 1C and 1D and Table S2). The chemical shifts in Ub arising from conjugation to Ubc13 are remarkably different than those observed for conjugation to UbcH5c, both in profile and magnitude (Figure 1D). The perturbations observed when Ubc13 is conjugated to Ub are not congruent with those expected for an E2~Ub complex in an extended state, as observed in the crystal structure of Ubc13-O~Ub.

The simplest interpretation of the observed perturbations is that they identify surfaces on Ubc13 and Ub that are in close proximity in the conjugate, suggesting a closed conformation in which the Ub is folded up towards the crossover helix of Ubc13. A similar closed state has been proposed for yeast Ubc1~Ub based on NMR observations (4), however because this E2~Ub was created using a wildtype thioester linkage, it suffered from a short half-life and incomplete NMR assignments. The chemical shift perturbations observed for the oxyester forms of UbcH5-O~Ub and Ubc13-O~Ub allow direct comparison and suggest that Ubc13-O~Ub populates closed conformations more frequently than does UbcH5c-O~Ub.

## Mapping the RING E3 binding surface of Ubc13 by Chemical Shift Perturbation Analysis

To determine an E3's ability to bind the closed Ubc13-O~Ub conformation, we measured CSPs for free Ubc13 and Ubc13-O~Ub upon the addition of 1.1 equivalents of the minimal RING domains of the heterodimeric RING E3 BRCA1/BARD1. The chemical shift perturbations on $^{15}$N-Ubc13 induced by BRCA1/BARD1 binding map to the conventional E3 binding surface comprised of Helix 1 and Loops 4 and 7 of Ubc13 (Fig 2b, Table S2 for residue level information). Resonances perturbed upon BRCA1/BARD1 addition to Ubc13-O~Ub map to the same surface as for free Ubc13. Conjugation-induced CSPs in Ubc13 residues (e.g., D44, T51) are not affected by E3 binding (Fig. 2A). These observations indicate that E3 binding does not preclude or detectably perturb the closed conformation of Ubc13-O~Ub.

## E2~Ub species are highly dynamic

To observe the resonances of the E2 and Ub moieties simultaneously, UbcH5c-O~Ub and Ubc13-O~Ub conjugates were generated using $^{15}$N-labeled E2 and $^{15}$N-labeled Ub. The $^{1}$H, $^{15}$N-HSQC-TROSY spectra of the resulting species display two classes of resonances distinguished by sharper peaks with higher intensities or broader peaks with lower intensities. NMR linewidths are a function of $T_2$ relaxation and therefore reflect the dynamics of individual groups within a protein. An E2~Ub conjugate in which both proteins behave as a globular complex would be expected to display similar linewidths throughout the spectrum. In both UbcH5c-O~Ub and Ubc13-O~Ub, the sharper, more intense resonances arise from the 8.6 kDa Ub subunit (Figure 3A), consistent with Ub behaving as a flexibly tethered protein that is largely independent of the 17 kDa E2 to which it is conjugated.

$T_1$ and $T_2$ relaxation times were measured for UbcH5c, Ub, and UbcH5c-O~Ub (Figure 3B). Within the conjugate, $T_1/T_2$ ratios differed significantly between the UbcH5c and Ub moieties (average values: 26.3 and 14.7, respectively). Average $T_1/T_2$ values for free UbcH5c and Ub were measured to be 9.2 and 3.3, respectively. The lifetime of the Ubc13-O~Ub oxyester conjugate (half life at pH 7 and 25°C ~10 hours) did not allow for collection of high quality $^{15}$N-T1 and $T_2$ relaxation measurements. In summary, both observed linewidths and $^{15}$N relaxation parameters indicate that the Ub moieties within the UbcH5-O~Ub and Ubc13-O~Ub conjugates behave as highly flexible entities independent of the E2s to which they are attached.

## Investigation of the solution conformations of E2~Ub: use of spin-labeled Ub

While the asymmetric CSPs observed for UbcH5c-O~Ub seem consistent with the dynamic behavior evidenced by the linewidths, the implied closed conformations for Ubc13-O~Ub based on CSPs seem contradictory to its dynamic behavior. The dynamics indicate that while Ubc13~Ub may populate a closed conformation that gives rise to the observed CSPs, this conformation must be in equilibrium with others, on a timescale that is consistent with the sharper linewidths for Ub. Exploiting the lack of cysteines in wild-type Ub, site-specific cysteine mutations were used to incorporate a thiol-reactive paramagnetic nitroxide probe

into Ub at positions 11 (K11SL), 39 (D39SL), 48 (K48SL), and 63 (K63SL). A spin label accelerates the T2 relaxation rate of nearby nuclei, resulting in broadening of linewidths in an HSQC-type NMR spectrum, referred to as the paramagnetic relaxation effect (PRE). The large magnitude of the paramagnetic effect provides sufficient sensitivity to allow for the observation of structures that are either transient or lowly populated, making it an excellent approach for studying the dynamic E2~Ub species.

### PRE experiments recapitulate the UbcH5c – Ub non-covalent complex

Our intention was to observe line broadening effects of spin-labeled Ub on an E2 to which it is conjugated. In light of the dynamic behavior described above, we first sought to ascertain whether broadening effects are detectable in a short-lived, transient species. We used a previously characterized low-affinity (non-covalent) complex formed between wild-type UbcH5c and Ub as a test case (PDB ID 2FUH (14)). Ub-K48SL (1 molar eq.) was added to $^{15}$N-UbcH5c and HSQC-TROSY spectra were collected in the absence (“active”) and presence (“reduced”) of ascorbate. Peak intensities were measured in both spectra and the ratios of active/reduced intensities were used as indicators for residues in close proximity to the paramagnetic probe. A majority of UbcH5c resonances exhibit a ratio close to 1.0, indicating that these resonances are not affected by the spin label and confirming that there are no non-specific interactions between the spin label and the E2. The strongest effect is observed for UbcH5 residue G27, as this resonance is undetectable in the “active” spectrum. Residues that were significantly affected by the spin label were identified as those with ratios differing from the mean by more than one standard deviation. When mapped onto the 3-dimensional structure, the affected residues define a surface that coincides with what is expected based on the solution structure solved on the basis of observed NOEs (Figure 4A,Table S3) (15).

### Investigation of E2~Ub Conformations: E2~UbSL experiments indicate a range of conformations within the conjugate

HSQC-TROSY spectra were collected for active and ascorbate-reduced $^{15}$N-UbcH5c-O~UbSL (with the S22R mutation) and $^{15}$N-Ubc13-O~UbSL for each spin label position in Ub (residues 11, 39, 48, and 63). Spectra in which one molar equivalent of each UbSL was added but not conjugated to $^{15}$N-UbcH5c/Ubc13 were also collected as controls for potential inter-molecular spin label effects. In general, the E2 + Ub-SL spectra showed no spin label-affected peaks, with the exception of small effects observed on the “backside” of UbcH5c in the K48SL and K11SL cases, most likely a result of some residual noncovalent interaction with Ub despite the S22R mutation (see Methods). These small backside effects were also observed in UbcH5c-O~Ub experiments (Figure 5). Several lines of evidence confirm that the modification of Ub with TEMPO does not alter its structural or functional properties. First, Ub-K11SL functions equivalent to wild-type Ub in an *in vitro* ubiquitination assay with UbcH5c and BRCA1/BARD1 (Figure S1). Second, spectral overlays of reduced PRE experiments at all spin label positions show no significant differences in the E2 spectra (Figure S2).

Results for the four spin label positions in the UbcH5c-O~Ub and Ubc13-O~Ub conjugates are summarized in Table 1, and residue-level histograms of intensity ratios for each species are included as Figure S4. In every spectral pair, the measured intensity ratios averaged over all E2 resonances is close to 1.0, confirming a lack of non-specific intensity loss that might be expected to affect random surface residues to some extent. The average measured intensity ratios over all data sets is 0.98 for both E2s, indicating that the samples and spectra were well-matched and providing high confidence in the intensities measured. Of the four Ub spin label positions, K48 gives the strongest PRE in the context of UbcH5c-O~Ub, with a lowest intensity ratio of 0.2 for E2 residues E122 and R131, while labels at Ub positions

K11 and D39 give the strongest effects in the context of Ubc13-O~Ub, with lowest ratios of 0.25 for Ubc13 residues I108 and K82, A122, respectively (Table 1). Of particular note is the clear difference in the K63 position, which shows no significant effects in the context of UbcH5c-O~Ub but strong effects (lowest ratio is 0.1) in Ubc13-O~Ub. Given the concurrence among all the E2-O~Ub PRE data sets, we chose to use a global threshold of 0.7 as the intensity ratio below which significance was assigned (i.e., an intensity loss greater than 30% of a peak's original intensity). (Table S3).

## Comparison of E2~Ub conjugates

Each of the four spin label positions in the context of UbcH5c-O~Ub affect a unique set of resonances. Affected UbcH5 residues reside in the crossover helix, the active site and C-terminal helices, and Loop 6. No single orientation of Ub relative to UbcH5 can satisfy all the observations, consistent with the flexible nature of the conjugate. To satisfy all the PRE effects, the conjugated Ub moiety must swing *via* its flexible C-terminal residues from closed conformations in which it approaches the E2 crossover helix, through extended conformations in which it resides below the active site and C-terminal helices, and up to Loops 5 and 6 in "backbent" conformations (Figure 5, left). Considering the two sequential glycines at the Ub C-terminus, remarkably little "twisting" of ubiquitin's C-terminal tail is required to move among these radically different conformations. Like the UbcH5c-O~Ub conjugate, no single Ubc13-O~Ub conformation can satisfy all of the PRE-affected surfaces. Together, the four spin label positions suggest a similar Ub trajectory as in the UbcH5c-O~Ub conjugate, except that the Ub moiety must twist to enable its hydrophobic I44 surface to face the two sides of the E2, as indicated by the K48SL effect observed on both the C-terminal helices and the β-sheet (Figure 5, right).

## Small angle X-ray scattering (SAXS) of the E2~Ub conjugates confirms NMR-based models

SAXS curves were collected on samples of UbcH5c, $His_6$-Ubc13, UbcH5c-O~Ub, and $His_6$-Ubc13-O~Ub at 25°C (Figure 6 A, B). No concentration-dependent effects or radiation damage was observed. Preliminary analysis of SAXS curves offers information on the shape ($R_g$) and size ($D_{max}$) of the sample proteins. The two free E2s give similar values for $R_g$ and $D_{max}$ that are consistent with monomeric E2s based on their known structures. UbcH5c-O~Ub and $His_6$-Ubc13-O~Ub also give similar values for $R_g$ (23.0 Å and 23.7 Å, respectively) and $D_{max}$ (70 Å and 75 Å, respectively). A $D_{max}$ value of approximately 72 Å is predicted for the open conformation of Ubc13-O~Ub observed in the crystal structure (2GMI). Thus, the SAXS data indicate that extended conformations are populated in solution both by Ubc13~Ub and UbcH5c~Ub.

We reasoned the five atomic-level structures of E2~Ub species (or their mimics) available in the PDB may represent a sampling of the allowable conformations available to E2~Ubs. Therefore, the structures were used as a basis set for further analysis of the SAXS data. Theoretical scattering curves were generated for each of the five E2~Ub structures using the programs CRYSOL and OLIGOMER for comparison with the measured curves for UbcH5c-O~Ub and Ubc13-O~Ub (Figure S5). Not surprisingly, no single structure produced a theoretical scattering curve that fits the experimental data (Figure S6A). Furthermore, no linear combination of 2, 3, 4, or 5 conformations chosen from a pool of existing E2~Ub structures could recapitulate the experimental curves (OLIGOMER; Figure 6 A, B). Among all possible combinations, conformations from the 2KJH and 1FXT structures fit the UbcH5c~Ub experimental data with $\chi^2$=5.45, while conformations of the Ubc13~Ub conjugate from the 3JW0 and 1FXT structures fit the data with $\chi^2$=3.87 (Figure S6B). Flexible systems such as the E2~Ub conjugate, however, likely populate a continuum of conformations that may differ from existing solved structures.

To better account for the flexibility of the E2~Ub conjugate, an ensemble optimization method (RanCh/GAJOE) was used to search for a minimal ensemble of UbcH5c~Ub orientations that recapitulate the experimental data. Our initial analysis of UbcH5c-O~Ub was based upon a 20-member ensemble (generated from a pool of 10,000 random conformations; see Experimental Methods) and included Ub orientations ranging from a closed state in which Ub is proximal to the E2 crossover helix, to an extended or open state in which Ub hangs below the E2 active site and C-terminal helices, to a backbent state in which Ub has swung to the opposite face of the E2 and is proximal to Loops 5 and 6 ($\chi^2$ value of 2.26; Figure 6A). The ensemble shows a slight preference for extended E2~Ub conformations, consistent with the weak CSPs observed in Ub upon conjugation to UbcH5c.

In contrast to the UbcH5~Ub ensemble, a 20-member Ubc13~Ub ensemble contains more conformers that represent a closed conformation with additional conformations that include the extended state and a weakly populated conformation placing Ub near the surface of Ubc13 that also binds Mms2 ($\chi^2$ value of 2.75), see Figure 6 B. The highly populated closed state observed in the SAXS ensemble coincides with the CSPs observed upon Ubc13~Ub conjugation.

In both cases, the ensembles of 20 E2~Ub models represent one possible set of conformations that fit the data and fine structural details should be analyzed in that light. Repeating the calculations to obtain additional ensembles, however, resulted in similar trends for both the pattern and density of E2~Ub orientations, with associated $\chi^2$ values remaining consistent in each case (Figure S6C). Furthermore, calculated ensembles comprised of fewer models yielded similar trends in E2~Ub conformations and comparable $\chi^2$ values (Figure S6D and E). Ensembles comprised of fewer than five structures were unable to satisfy both the pattern and density of E2~Ub models observed in larger ensembles and, as a result, yielded poorer $\chi^2$ values. Although there is little statistical difference between ensembles containing five or twenty models, we believe that a twenty-member ensemble better reflects properties of an E2~Ub species as it reveals lowly-populated conformations.

## DISCUSSION

E2~Ub species are essential components of the multi-protein complex required for the transfer of Ub to substrates. Several recent crystal structures and static NMR-based models have significantly increased the structural information available, but the solution-state behavior of E2~Ubs reported here and previously by other groups (22) (23) suggest that such structures provide a snapshot of what is a conformationally dynamic species. Here we present a more comprehensive description of the conjugate forms of two human E2s, UbcH5c and Ubc13, and find distinct differences between the two closely related E2s.

The NMR spectral features of both UbcH5c~Ub and Ubc13~Ub are consistent with flexibly linked domains, as indicated by linewidth analysis and $^{15}$N relaxation data. Chemical shift perturbations, paramagnetic relaxation enhancement, and small angle X-ray scattering identify distinct features of the two E2~Ub species. Despite the strong CSPs observed in Ubc13 and Ub upon conjugation, analyses of linewidth, PRE, and SAXS data indicate a flexible species that inhabits multiple E2~Ub conformations. Chemical shift perturbations suggest that the preferred state of the flexibly linked Ub is folded up towards the crossover helix of Ubc13, in what we call the closed conformer. Notably, the Ub swings “backwards” toward loop 4 and β-strand 4 of Ubc13 more rarely than it swings up into the closed conformation, based upon SAXS and CSP data. This is in contrast to UbcH5c~Ub, which appears to prefer a more open state, based on analysis of SAXS data and the general lack of Ub CSPs upon activation. Another notable difference is in Ub’s C-terminus: PRE data

indicate that the I44 hydrophobic face of Ub approaches both the front and back of Ubc13, implying that a twist in the Ub C-terminus must occur, whereas there is no evidence that the UbcH5c~Ub conjugate undergoes such a pronounced twist.

Currently, there are two deposited crystal structures of UbcH5~Ub. In one structure (PDB 3A33), the conjugated Ub is in a conformation similar to the backbent orientation included in the UbcH5c~Ub ensemble (6). The other is a structure of a complex formed between UbcH5b~Ub and the HECT-type E3, Nedd4L (7). In this case, the conjugated Ub is in an extended-twisted conformation that places Ub residue D39 near UbcH5 Loop 8, a state that is also included in the UbcH5c~Ub ensemble. These structures suggest how additional binding interactions may select a particular E2~Ub conformation from among manifold possibilities.

The conjugation-induced CSPs in human Ubc13 agree with a previous report (24), although our complete $^{15}N$-$^{1}H$ assignments afford a more detailed view of the Ubc13~Ub species. An extended state of Ubc13~Ub as observed in the crystal structure (PDB 2GMI) is represented among the conformations in the solution ensemble. The presence of Ubc13 binding partner, Mms2, which can interact with a Ub moiety from another Ubc13~Ub conjugate, may shift the equilibrium towards the extended state seen in the crystal. It is beyond the technical scope of the present study to characterize the conjugated Ubc13/Mms2 heterodimer in solution, so we cannot comment further on the effects of Mms2 binding. Overall, our results indicate that Ubc13~Ub populates a closed state with highest frequency. Furthermore, our NMR data indicate that binding of the RING E3, BRCA1/BARD1 to Ubc13~Ub does not preclude the closed state observed in the ensemble.

There are a growing number of reports of proteins that selectively recognize E2~Ub conjugates, but not the free protein components. To date, three proteins have been identified that specifically bind an E2~Ub conjugate: bacterial E3 ligase SspH2 (binds UbcH5c~Ub) (23), bacterial effector protein OspG (binds UbcH5b~Ub) (25), and nuclear import protein importin-11 (binds UbcM2~Ub) (26). Ub and E2 enzymes individually contain a number of potential binding sites; conjugation of the two proteins creates new combinatorial possibilities that may create unique binding modes. Based on the two crystal structures available, it appears that (at least in these cases) interacting proteins make use of available E2~Ub orientations in their modes of binding. Multiple conformations assumed by the E2~Ub conjugate allow for diverse binding modes. Such flexibility allows the E2~Ub conjugate to participate in a variety of complexes, ultimately resulting in diverse biological roles. Commonalities among E2~Ub structures might be related to common binding partners. For example, neither the Ubc13~Ub model nor the UbcH5c~Ub model place Ub in an orientation that is likely to interfere with binding to a RING E3. On the other hand, differences in E2~Ub structures could be linked to differences in binding partners, including non-canonical E3 ligases. As a result, studying molecular interactions with the free E2 may not directly translate to the E2~Ub conjugate.

Despite the technical challenges posed, it is clear that studying the active, conjugated form of E2 Ub-conjugating enzymes can provide insights not readily apparent from the structures of isolated E2s. Understanding the combinatorial effect of E2 and Ub binding sites and the E2-specific conformational ensembles will be key to deciphering the E2 protein interactome. The NMR-based spin labeling approach described herein will be generally applicable to the study of other E2~Ub conjugates as well as to E2~Ub species in complex with interacting proteins, including E3 ligases.

## Supplementary Material

Refer to Web version on PubMed Central for supplementary material.

## Acknowledgments

We thank SSRL and PNNL for beam time and the use of magnets. Portions of this research were carried out at the Stanford Synchrotron Radiation Laboratory Beamline 4-2, a national user facility operated by Stanford University on behalf of the U.S. Department of Energy, Office of Basic Energy Sciences. The SSRL Structural Molecular Biology Program is supported by the Department of Energy, Office of Biological and Environmental Research, and by the National Institutes of Health, National Center for Research Resources, Biomedical Technology Program. A portion of the research was performed using EMSL, a national scientific user facility sponsored by the Department of Energy's Office of Biological and Environmental Research and located at Pacific Northwest National Laboratory. We gratefully acknowledge Walter Chazin and members of the Klevit lab for helpful discussions and critical reading of the manuscript.

Funding Information: This work was supported by NIH grant R01 GM088055 (R.E.K.), PHS NRSA T32 GM008268 (K.E.S. and J.N.P.), and PHS NRSA 2T32 GM007270 from NIGMS (J.N.P.).

## Abbreviations

| | |
|---|---|
| **Ub** | ubiquitin |
| **E2** | ubiquitin-conjugating enzyme |
| **E3** | ubiquitin ligase |
| **E1** | ubiquitin-activating enzyme |
| **RING** | Really Interesting New Gene |
| **HECT** | Homologous to E6AP Carboxy Terminus |
| **NMR** | nuclear magnetic resonance |
| **SAXS** | small angle x-ray scattering |
| **PRE** | paramagnetic relaxation enhancement |

## REFERENCES

1. Pickart CM. Mechanisms underlying ubiquitination. Annu Rev Biochem 2001;70:503–533. [PubMed: 11395416]
2. Ye Y, Rape M. Building ubiquitin chains: E2 enzymes at work. Nat Rev Mol Cell Biol 2009;10:755–764. [PubMed: 19851334]
3. Eddins MJ, Carlile CM, Gomez KM, Pickart CM, Wolberger C. Mms2-Ubc13 covalently bound to ubiquitin reveals the structural basis of linkage-specific polyubiquitin chain formation. Nat Struct Mol Biol 2006;13:915–920. [PubMed: 16980971]
4. Hamilton KS, Ellison MJ, Barber KR, Williams RS, Huzil JT, McKenna S, Ptak C, Glover M, Shaw GS. Structure of a conjugating enzyme-ubiquitin thiolester intermediate reveals a novel role for the ubiquitin tail. Structure 2001;9:897–904. [PubMed: 11591345]
5. Serniwka SA, Shaw GS. The structure of the UbcH8-ubiquitin complex shows a unique ubiquitin interaction site. Biochemistry 2009;48:12169–12179. [PubMed: 19928833]
6. Sakata E, Satoh T, Yamamoto S, Yamaguchi Y, Yagi-Utsumi M, Kurimoto E, Tanaka K, Wakatsuki S, Kato K. Crystal structure of UbcH5b~ubiquitin intermediate: insight into the formation of the self-assembled E2~Ub conjugates. Structure 2010;18:138–147. [PubMed: 20152160]
7. Kamadurai HB, Souphron J, Scott DC, Duda DM, Miller DJ, Stringer D, Piper RC, Schulman BA. Insights into ubiquitin transfer cascades from a structure of a UbcH5B~ubiquitin-HECT(NEDD4L) complex. Mol Cell 2009;36:1095–1102. [PubMed: 20064473]

8. Ozkan E, Yu H, Deisenhofer J. Mechanistic insight into the allosteric activation of a ubiquitin-conjugating enzyme by RING-type ubiquitin ligases. Proc Natl Acad Sci USA 2005;102:18890–18895. [PubMed: 16365295]
9. Huang A, de Jong RN, Wienk H, Winkler GS, Timmers HTM, Boelens R. E2-c-Cbl recognition is necessary but not sufficient for ubiquitination activity. J Mol Biol 2009;385:507–519. [PubMed: 18996392]
10. Siepmann TJ, Bohnsack RN, Tokgöz Z, Baboshina OV, Haas AL. Protein interactions within the N-end rule ubiquitin ligation pathway. J Biol Chem 2003;278:9448–9457. [PubMed: 12524449]
11. Haas AL, Rose IA. The mechanism of ubiquitin activating enzyme. A kinetic and equilibrium analysis. J Biol Chem 1982;257:10329–10337. [PubMed: 6286650]
12. Michelle C, Vourc'h P, Mignon L, Andres CR. What was the set of ubiquitin and ubiquitin-like conjugating enzymes in the eukaryote common ancestor? J Mol Evol 2009;68:616–628. [PubMed: 19452197]
13. Moraes TF, Edwards RA, McKenna S, Pastushok L, Xiao W, Glover JNM, Ellison MJ. Crystal structure of the human ubiquitin conjugating enzyme complex, hMms2-hUbc13. Nat Struct Mol Biol 2001;8:669–673.
14. Brzovic PS, Keeffe JR, Nishikawa H, Miyamoto K, Fox D 3rd, Fukuda M, Ohta T, Klevit R. Binding and recognition in the assembly of an active BRCA1/BARD1 ubiquitin-ligase complex. Proc Natl Acad Sci USA 2003;100:5646–5651. [PubMed: 12732733]
15. Brzovic PS, Lissounov A, Christensen DE, Hoyt DW, Klevit RE. A UbcH5/ubiquitin noncovalent complex is required for processive BRCA1-directed ubiquitination. Mol Cell 2006;21:873–880. [PubMed: 16543155]
16. Delaglio F, Grzesiek S, Vuister GW, Zhu G, Pfeifer J, Bax A. NMRPipe: a multidimensional spectral processing system based on UNIX pipes. J Biomol NMR 1995;6:277–293. [PubMed: 8520220]
17. Johnson BA, Blevins RA. NMR View: A computer program for the visualization and analysis of NMR data. J Biomol NMR 1994;4:603–614.
18. Konarev PV, Volkov VV, Sokolova AV, Koch MHJ, Svergun DI. PRIMUS: a Windows PC-based system for small-angle scattering data analysis. J Appl Crystallogr 2003;36:1277–1282.
19. Svergun DI. Determination of the regularization parameter in indirect-transform methods using perceptual criteria. J Appl Crystallogr 1992;25:495–503.
20. Svergun D, Barberato C, Koch MHJ. CRYSOL - a Program to Evaluate X-ray Solution Scattering of Biological Macromolecules from Atomic Coordinates. J Appl Crystallogr 1995;28:768–773.
21. Bernadó P, Mylonas E, Petoukhov MV, Blackledge M, Svergun DI. Structural Characterization of Flexible Proteins Using Small-Angle X-ray Scattering. J Am Chem Soc 2007;129:5656–5664. [PubMed: 17411046]
22. Miura T, Klaus W, Gsell B, Miyamoto C, Senn H. Characterization of the binding interface between ubiquitin and class I human ubiquitin-conjugating enzyme 2b by multidimensional heteronuclear NMR spectroscopy in solution. J Mol Biol 1999;290:213–228. [PubMed: 10388568]
23. Levin I, Eakin C, Blanc M-P, Klevit RE, Miller SI, Brzovic PS. Identification of an unconventional E3 binding surface on the UbcH5 ~ Ub conjugate recognized by a pathogenic bacterial E3 ligase. Proc Natl Acad Sci USA 2010;107:2848–2853. [PubMed: 20133640]
24. McKenna S, Moraes T, Pastushok L, Ptak C, Xiao W, Spyracopoulos L, Ellison MJ. An NMR-based model of the ubiquitin-bound human ubiquitin conjugation complex Mms2.Ubc13. The structural basis for lysine 63 chain catalysis. J Biol Chem 2003;278:13151–13158. [PubMed: 12569095]
25. Kim DW, Lenzen G, Page A-L, Legrain P, Sansonetti PJ, Parsot C. The Shigella flexneri effector OspG interferes with innate immune responses by targeting ubiquitin-conjugating enzymes. Proc Natl Acad Sci USA 2005;102:14046–14051. [PubMed: 16162672]
26. Plafker SM, Plafker KS, Weissman AM, Macara IG. Ubiquitin charging of human class III ubiquitin-conjugating enzymes triggers their nuclear import. J Cell Biol 2004;167:649–659. [PubMed: 15545318]

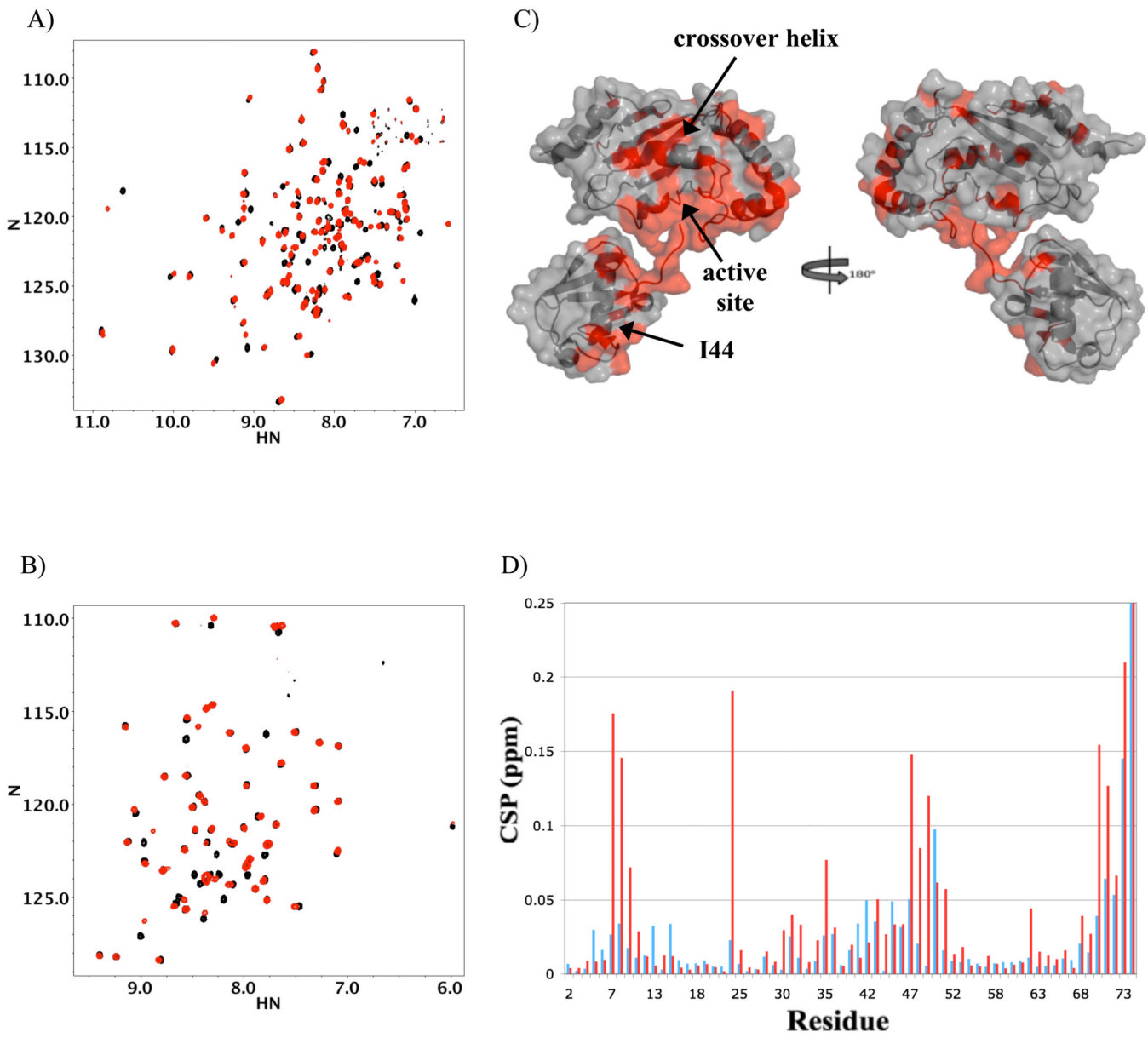


**Figure 1.**

Spectral perturbations observed in Ubc13 and Ub upon formation of Ubc13-O~Ub conjugate. A) 2D HSQC-TROSY spectrum of $^{15}$N-Ubc13 (black) is overlaid with spectrum of oxy-ester linked $^{15}$N-Ubc13-O~Ub (red). B) 2D HSQC-TROSY spectrum of $^{15}$N-Ub (black) is overlaid with $^{15}$N-Ub~O-Ubc13 (red). C) Combined $^{1}$H and $^{15}$N chemical shift perturbations greater than 0.05 ppm are mapped in red onto the structure of conjugated Ubc13-O~Ub (PDB code 2GMI with human Ubc13 structure overlaid PDB code 1J7D). Perturbations reveal surfaces on both Ubc13 and Ub, suggestive of a protein-protein interaction in which the hydrophobic I44 surface of Ub rotates to meet the surface mapped on Ubc13. D) Histogram showing Ub CSPs upon activation to Ubc13 (red) and UbcH5c (blue). Comparison of the two profiles reveals differences in both the identity of affected residues and the degree to which they are perturbed.

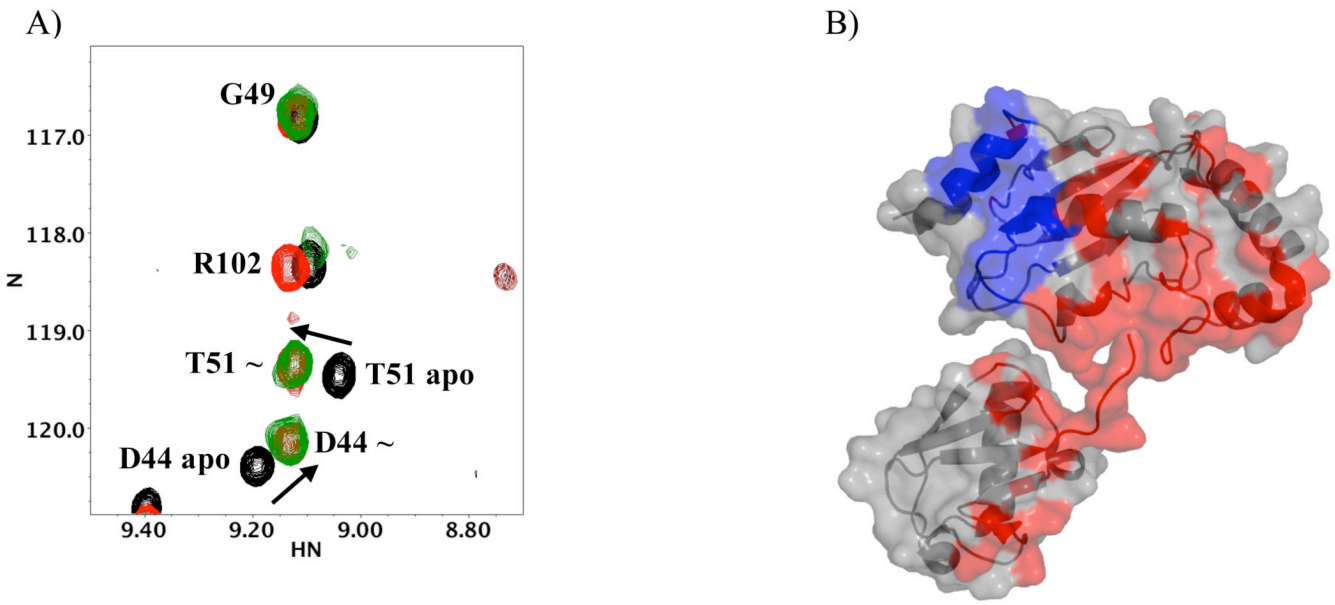


**Figure 2.**

E3 binding does not disrupt the closed state. A) 2D HSQC-TROSY spectrum of $^{15}$NUbc13 (black) is overlaid with $^{15}$N-Ubc13-O~Ub (red) and with $^{15}$N-Ubc13-O~Ub plus 1.1 mol. equiv. BRCA1 1–112/BARD1 1–114 RING domains (green). Ubc13 residues D44 and T51 which are perturbed upon conjugation with Ub are not affected by BRCA1 binding to the E2~Ub conjugate, indicating Ubc13~Ub can adopt the closed conformation even when bound to BRCA1. B) CSP greater than 0.05 ppm upon the addition of 1.1 equivalent RING E3 BRCA1/BARD1 are mapped in blue onto the structure of conjugated Ubc13~Ub (PDB code 2GMI with human Ubc13 structure overlaid PDB code 1J7D). CSPs upon conjugation to Ub as in Figure 1C are mapped in red.

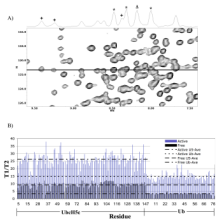

**Figure 3.**
NMR resonance linewidths and intensities indicate that the E2~Ub conjugate is a dynamic species. A) 2D HSQC-TROSY spectrum of $^{15}$N-Ubc13-O~$^{15}$N-Ub shows two classes of peaks based on intensity. In general, peaks that are sharper (more intense) arise from Ub residues, while the broader (weaker) peaks arise from Ubc13 residues. A 1D slice taken at the $^{15}$N frequency denoted by the black horizontal line in the 2D spectrum illustrates the distinction between Ub (*) and Ubc13 (+) resonances. A limited number of more intense Ubc13 resonances are observed (Δ); these arise from residues in loops or near the C-terminus. Off-center peaks are not labeled. B) Histogram of $T_1/T_2$ values for UbcH5c and Ub residues in their conjugated (blue) and free (black) forms.

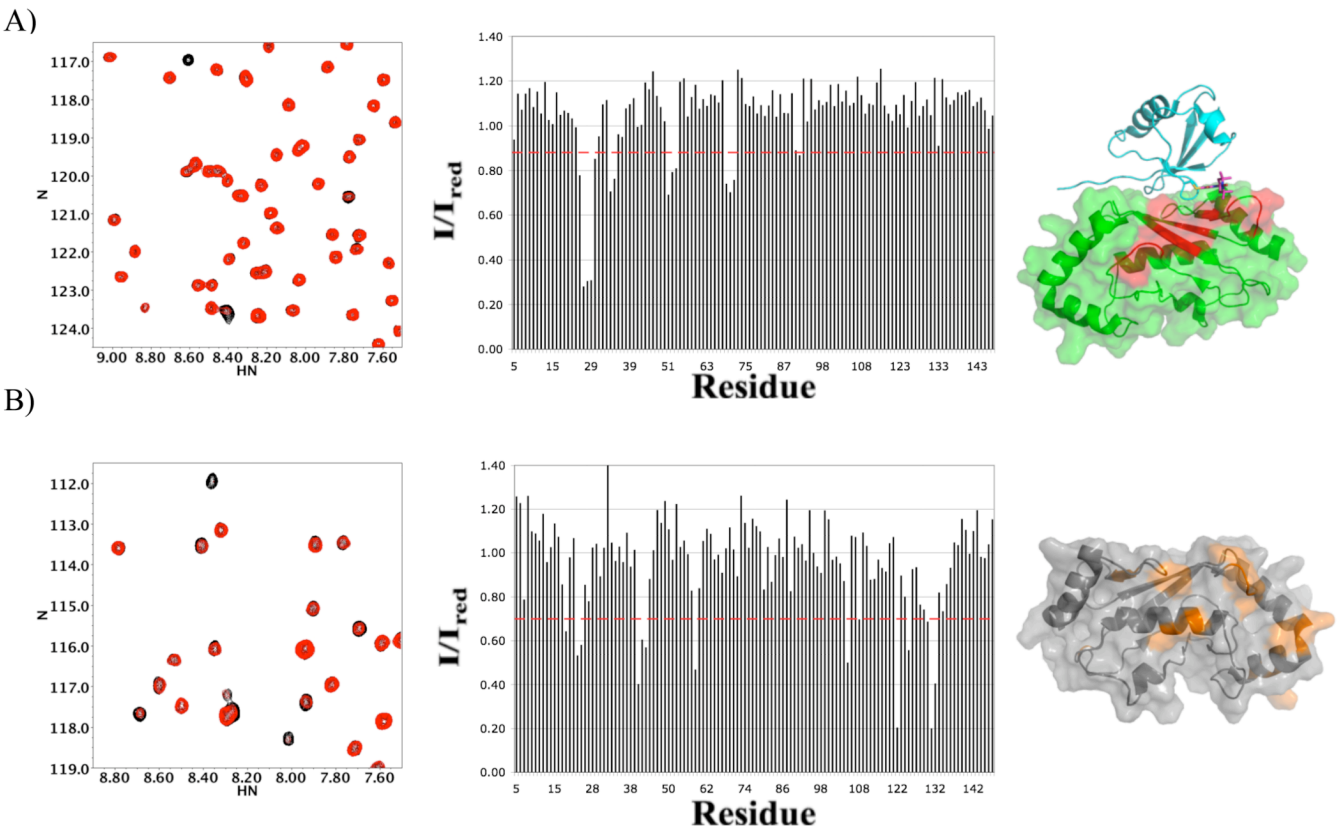


**Figure 4.**

Paramagnetic Relaxation Enhancement data analysis. A) 2D HSQC-TROSY spectra were taken of $^{15}$N-UbcH5c with 1 molar equiv. of Ub-K48SL before (red) and after reduction with ascorbate (black, left). Peak intensities were measured and plotted as ratios of $I/I_{red}$ (center). Residues corresponding to intensity ratios lower than one standard deviation from the mean were mapped onto the 3-D structure (right). B) As in A) for the $^{15}$N-UbcH5c-O~Ub-K48SL experiment.

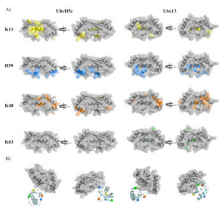

**Figure 5.**

Observed PREs are specific to both spin label position and E2 identity. A) Highlighted residues in UbcH5c (2FUH, left) and Ubc13 (1J7D, right) are those whose resonances show PRE effects upon conjugation with Ub-SL at positions K11 (yellow), D39 (blue), K48 (orange), and K63 (green). Colored residues correspond to HSQC peaks with an $I/I_{red}$ intensity ratio of ≤0.7. B) Illustrative extreme E2~Ub conformations. SL positions shown as colored spheres to match affected regions shown above, Ub core C-terminus and E2 active sites shown as gray spheres.

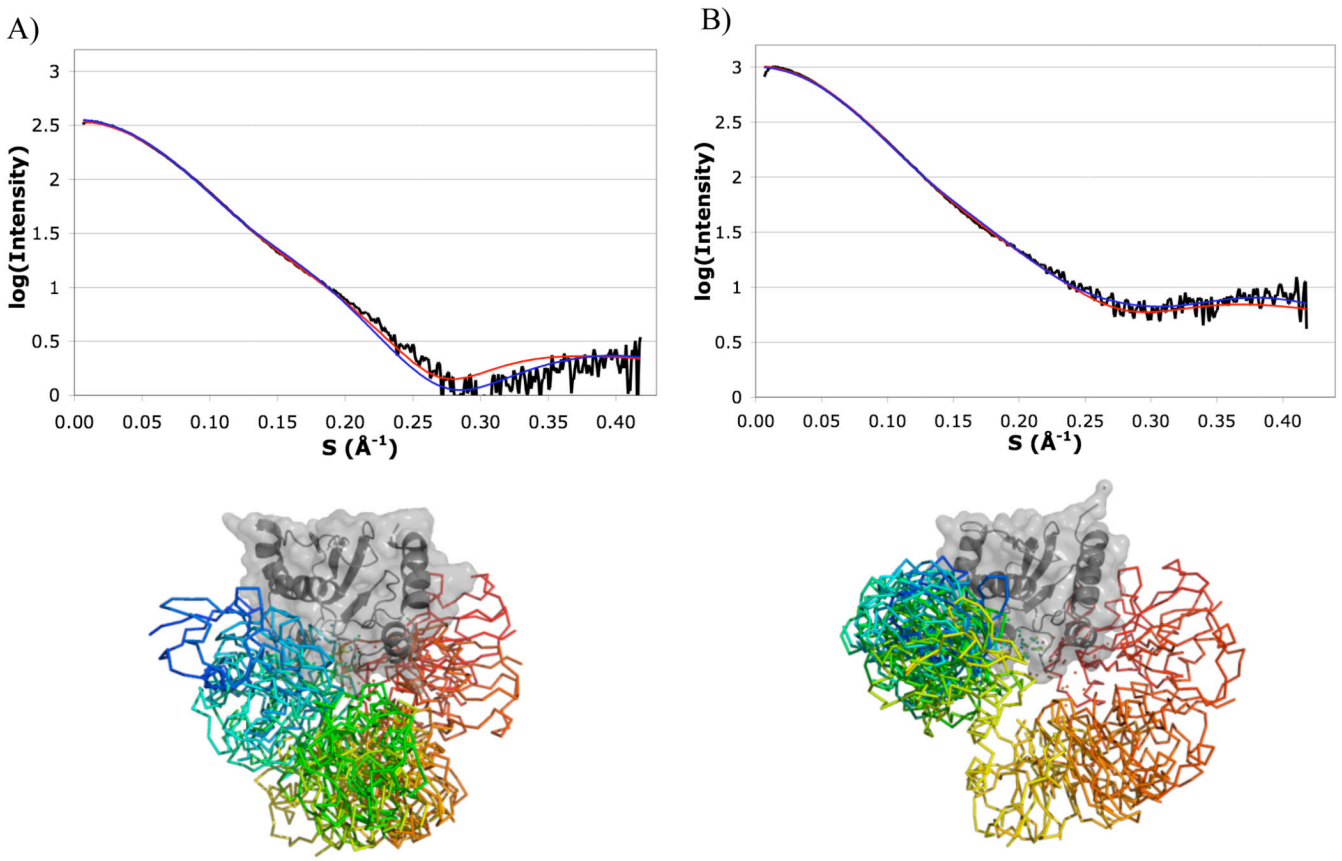


**Figure 6.**

Analysis of SAXS curves reveals a range of E2~Ub conformations. A) Experimental SAXS data of the UbcH5c-O~Ub conjugate (upper, black) overlaid with calculated fits produced from OLIGOMER (blue, based on 5 published E2~Ub structures) and EOM (red; RanCh/GAJOE) analysis. Ensemble of 20 UbcH5c~Ub conformations produced by EOM analysis is shown (lower). B) As in A) for the Ubc13-O~Ub conjugate.

**Table 1**

Comparison of the spin label effects between UbcH5c-O~Ub, Ubc13-O~Ub, and UbcH5c + Ub.

| UbcH5c-O~Ub | Ave. $I/I_{red}$ Ratio | STDEV | Lowest $I/I_{red}$ Ratio | Res. w/lowest $I/I_{red}$ ratio | # of Significant Residues |
|---|---|---|---|---|---|
| K11SL | 0.9 | 0.22 | 0.36 | 109 | 21 |
| D39SL | 0.9 | 0.22 | 0.38 | 84 and 87 | 23 |
| K48SL | 0.96 | 0.22 | 0.2 | 122 and 131 | 14 |
| K63SL | 1.14 | 0.12 | 0.86 | 94 | 0 |
| **Ubc13-O~Ub** | | | | | |
| K11SL | 0.93 | 0.16 | 0.25 | 108 | 8 |
| D39SL | 0.88 | 0.22 | 0.25 | 82, 122 | 18 |
| K48SL | 0.96 | 0.21 | 0.38 | 134 | 17 |
| K63SL | 1.13 | 0.2 | 0.1 | 149 | 4 |
| **UbcH5c+Ub** | | | | | |
| K48SL | 1.06 | 0.2 | 0.28 | 26 | 14 |